

Radio halo formation through magneto-turbulent particle acceleration in clusters of galaxies

Hiroshi Ohno ¹, Motokazu Takizawa ^{2,3}, and Shinpei Shibata ²

ABSTRACT

We developed a magneto-turbulent model for the cosmic ray (CR) electrons seen in the radio halo clusters of galaxies. Steady state momentum distribution functions of the CR electrons are calculated for given spectra of the turbulent Alfvén waves. The radio spectrum produced by the obtained CR electron distribution is compared to the observed radio spectrum of the Coma radio halo. We find that the observed radio spectrum of the Coma cluster is well reproduced when the spectral index of the turbulent Alfvén waves is ~ 2.8 . The obtained energy spectrum of the turbulent Alfvén waves is steeper than that expected from the turbulence theory, suggesting back reaction of the particle acceleration. The fitting procedure constraints the amplitude of the turbulent Alfvén waves as well as the spectral index. Then we estimate the dissipation of the turbulent Alfvén waves, which is found to be less than the cooling rate by X-ray radiation. We suggest that the turbulence which is sufficient for particle acceleration is developed in the clusters containing the radio halo. It is most likely that cluster mergers create the turbulence and seed relativistic electrons.

Subject headings: acceleration of particles – galaxies: clusters: general – intergalactic medium – radiation mechanisms: non-thermal

1. INTRODUCTION

The radio halo in a cluster of galaxies is a diffuse nonthermal (synchrotron) radio emission seen in the central region of ~ 1 Mpc in diameter. According to Hanisch (1982), the typical luminosity is $L_t \sim 10^{40} - 10^{41}$ erg s $^{-1}$ (10 MHz $\leq \nu \leq 10$ GHz), and the spectral

¹Yamagata Junior College, Yamagata, 990-2316, Japan; ohno@yamagata-jc.ac.jp

²Department of Physics, Yamagata University, Yamagata, 990-8560, Japan; takizawa@ksirius.kj.yamagata-u.ac.jp, shibata@ksirius.kj.yamagata-u.ac.jp

³Department of Astronomy, University of Virginia, P.O. Box 3818 Charlottesville, VA 22903-0818

index is $1 \lesssim \alpha \lesssim 2$. The typical spatial scale of the radio halos is larger than the optical core radius, but smaller than the Abell radius. Giovannini, Tordi, & Feretti (1999) inspected a sample of 205 clusters from the X-ray-brightest Abell-type clusters (Ebeling et al. 1996) to search for new radio halo and relic candidates. They found only 29 candidates. In addition, they found that occurrence of the radio halos and relics is higher in clusters with higher X-ray luminosity and higher temperature and confirmed that the positive correlation between the absence of a cooling flow and the presence of radio halo. The rarity of the radio halo is one characteristic to be considered in its formation scenario.

In clusters of galaxies with radio halos, nonthermal X-ray radiation due to inverse Compton scattering of cosmic microwave background (CMB) photons is expected (Rephaeli 1979). Indeed, nonthermal hard X-ray radiation was recently detected in a few rich clusters (e.g., Fusco-Femiano et al. 1999; Rephaeli, Gruber, & Blanco 1999; Fusco-Femiano et al. 2000) and several galaxy groups (Fukazawa 2001), although their origin is still unidentified.

Among clusters with radio halo, the Coma cluster is the most informative. The halo size is $30' - 40'$ in diameter corresponding to $600 - 800 h_{100}^{-1}$ kpc. The radio halo region contains two bright radio galaxies, NGC4874 and NGC4869. The spatially averaged spectral index of the halo, with reduction of contamination by the radio galaxies, is $\alpha \sim 1.3$. Giovannini et al. (1993) presented a spatial distribution of the spectral index between 326 MHz and 1.4 GHz. They found that the radio spectrum of the central halo region with size of $\sim 15'$ is flatter, $\alpha \sim 0.8$, while in the vicinity of the tailed radio source associated with NGC4869 is steeper, $\alpha \sim 1.8$. This means that high energy cosmic rays (CRs) are more abundant in the halo region than in the vicinity of the tailed source. The flatness of the radio halo spectrum suggests particle acceleration in the intracluster space. This has been pointed out by Giovannini et al. (1993). The radio spectrum of the outer region of the radio halo is steeper ($\alpha \sim 1.8$) than that of the central region.

Kim et al. (1990) studied the magnetic fields in the Coma cluster by using the rotation measures (RMs) of background radio sources (QSO and radio galaxies). The observed RMs of the background sources seen through the Coma cluster have an excess of ~ 38 rad m $^{-2}$. By adopting a galaxy scale of 10–40 kpc as a correlation length, they found the (electron density weighted) amplitude of the random magnetic field to be $\sim 1 \mu\text{G}$. On the other hand, the comparison between nonthermal hard X-ray emission and synchrotron radio emission gives the volume averaged magnetic field strength, if all the hard X-ray is emitted through inverse Compton scattering of CMB photons (Rephaeli 1979). Rephaeli, Gruber, & Rothschild (1987) obtained a lower limit value $\sim 0.11 \mu\text{G}$ by using the upper limit on the hard X-ray emission from the Coma cluster. The first detection of the hard X-ray emission from the Coma cluster by *BeppoSAX* gives the field strength of $0.15 \mu\text{G}$ (Fusco-Femiano et al. 1999).

The obtained values are significantly smaller than those derived from RMs. However, it is important to note that (1) these estimates assume that the emitting volumes of the hard X-ray and radio emission coincide, which might not be guaranteed, and that (2) these estimates are affected by the presence of additional infrared background radiation fields (Schlickeiser & Rephaeli 1990). These simplification can make the derived field strength smaller than that derived from RMs.

The origin of the CR electrons in the clusters with radio halo is still unclear. Jaffe (1977) proposed the primary electron model where the radio halo is an emission by CR electrons diffusing away from radio galaxies in a cluster. However, this model contains some difficulties, one of which is that the diffusion distance does not seem as large as the radio halo extent. Dennison (1980) proposed the secondary electron model where the relativistic electrons are produced through decay of charged pions induced by the interaction between relativistic protons from radio galaxies and thermal protons in ICM. In this model, however, too much gamma-ray emission is produced at least for the Coma cluster (Blasi & Colafrancesco 1999).

Excess of the high energy CR electrons in the halo region, indicated by the flat spectrum, strongly suggests the particle acceleration in an intracluster space. Models considering particle acceleration by intracluster magnetic turbulence were discussed by Roland (1981), Schlickeiser, Sievers, & Thiemann (1987), and Petrosian (2001). In this paper, we model the radio halo in terms of particle acceleration by the intracluster turbulent magnetic fields. The turbulence is assumed to be an ensemble of Alfvén waves, and the CR electrons are accelerated by pitch angle scattering by the Alfvén waves. Distribution functions of the CR electrons in energy space are obtained by solving a Fokker-Planck equation for the assumed turbulent spectra with various power indices. The calculated radio spectra are compared with the observed one to determine the energy spectrum of the turbulent Alfvén waves.

Deiss et al. (1997) proposed a merger shock acceleration model which explains the rarity of radio halos. Numerical simulations by Takizawa & Naito (2000) show radio emission is luminous while merger shocks accelerate CR electrons but decrease rapidly because of inverse Compton cooling after the shocks disappear. The transient feature of this model is consistent with the rarity of radio halos. We will discuss the relation between our model and theirs.

In §2, the basic equations to calculate a radio spectrum are introduced. In §3, the calculated spectra are interpreted, and the energy spectra of the turbulent Alfvén waves is determined so as to reproduce the observed radio spectrum. In §4, the generation mechanism of the obtained energy spectra is investigated, and over all turbulence structure is discussed. §5 is for summary.

2. MODEL

2.1. Resonant Acceleration by Turbulent Alfvén Waves

Energy of CR electrons is gained through a number of pitch angle scattering by Alfvén waves (e.g., Wentzel 1974; Skilling 1975; Blandford & Eichler 1987; Berezinsky et al. 1990; Terasawa 1991). The resonance scattering condition for an electron of velocity along the magnetic field v_{\parallel} with a wave of a frequency ω_A and wave number k is

$$\omega_A = kv_{\parallel} + \Omega_e, \quad (1)$$

where Ω_e is the electron cyclotron frequency, and the Alfvén velocity relates ω_A and k by $\omega_A = kv_A$. This condition means that the electron travels with the Alfvén wave along the mean field at a locked phase. The wave number resonant with the CR electron of energy E is approximated as

$$|k_{\text{res}}| = \left| \frac{-\Omega_e}{\mu v - v_A} \right|, \quad (2)$$

where μ is the cosine of the pitch angle, $v \sim c$ is the CR electron velocity.

When $\mu \gg v_A/c$, $|k_{\text{res}}| \sim eB_0/E$, where e and E are the charge and the energy of the CR electron, and B_0 is the large-scale-field strength. The energy of the CR electron is $E \sim m_{e0}c^2\gamma$, where m_{e0} and γ are the rest mass and the Lorentz factor of the CR electron. For $E \gtrsim 100$ MeV, $k_{\text{res}} \lesssim 3 \times 10^{-12}B_{\mu\text{G}} \text{ cm}^{-1}$, where $B_{\mu\text{G}}$ is the large-scale-field strength in units of μG . In this wave number range, the magnetohydrodynamical description of the Alfvén wave is valid because $k \ll k_{\text{max}} \sim \Omega_i/v_i \sim 10^{-10} B_{\mu\text{G}} \text{ cm}^{-1}$, where v_i is the ion sound velocity (Holman, Ionson, & Scott 1979). This picture is not valid when μ is much less than v_A/c . When $\mu \sim 0$, the resonant wave number $k_{\text{res}} \sim eB_0/(m_e c \gamma v_A) \sim 10^{-8} \text{ cm}^{-1}$, which is larger than the k_{max} for 100 MeV electrons, and therefore well in the whistler or ion-cyclotron range. Steinacker & Miller (1992) discuss the gyroresonance of the electrons with parallel transverse cold plasma waves including the Alfvén waves, whistlers, and cyclotron waves, and derive the Fokker-Planck equation describing the evolution of the electron distribution function. Also, Felice & Kulsrud (2001) suggest that scattering at $\mu \sim 0$ is affected by transit-time damping effect with long-wavelength waves. These processes should be included in the model for the radio halos. For this we have to give energy spectra of all wave modes related to these processes to obtain diffusion coefficients. However, it is difficult to assume the energy spectra of all wave modes realistically because we do not have sufficient information about the generation mechanisms of the waves and the interaction between the waves. The aim of this paper is to evaluate the energy spectrum of the Alfvén waves accelerating the CR electrons producing the radio halo. Then we attempt to do this assuming that pitch angle scattering by Alfvén waves is dominant process, hoping corrections by other processes

near $\mu \sim 0$ is small. However, we must note that if the correction to the present form of diffusion coefficient by other wave modes is significant, our evaluation of the energy spectrum of the Alfvén wave mode would not be valid. In this paper, we adopt a pitch-angle averaged diffusion coefficient of the resonant scattering as a reasonably good approximation (Isenberg 1987; Schlickeiser 1989; Blasi 2000).

The energy spectrum of the turbulent Alfvén waves is assumed to be a single power law with an index $w > 1$:

$$P(k) = b \frac{B_0^2 (w-1)}{8\pi} \left(\frac{k}{k_0} \right)^{-w}, \quad k_0 \leq k \leq k_{\max}, \quad (3)$$

where the applicable range, $k_0 \leq k \leq k_{\max}$, is discussed later; the normalization factor b indicates the fractional energy density of the turbulent Alfvén waves if $k_{\max} \gg k_0$. In this case, the pitch angle-averaged momentum diffusion coefficient is given by

$$D_{\text{pp}} = (m_{\text{e}0} c)^2 a_1 \gamma^w, \quad (4)$$

where

$$a_1 = \frac{w-1}{w(w+2)} \pi b \frac{v_{\text{A}}}{c} k_0 v_{\text{A}} \gamma_0^{2-w}, \quad (5)$$

(Isenberg 1987; Schlickeiser 1989; Blasi 2000). Here the relation between γ and k is

$$k = \frac{e B_0}{m_{\text{e}0} c^2 \gamma}, \quad (6)$$

and γ_0 corresponds to k_0 . Also the spatial and momentum diffusion coefficients are related by

$$D_0 = \frac{v_{\text{A}}^2}{9} \frac{p^2}{D_{\text{pp}}}, \quad (7)$$

(Melrose 1980; Schlickeiser et al. 1987).

The transit-time damping effect of fast magnetosonic waves plays a more crucial role for lower energy ($\gamma < 1836$) electrons (Schlickeiser & Miller 1998; Ragot & Schlickeiser 1998), which will emit EUV radiation through inverse Compton scattering of CMB photons and possibly contribute in lower energy ends of the radio and hard X-ray emission. Therefore, this effect should be considered when broader energy band spectrum models are constructed.

2.2. Basic Equations

We simplify the problem as follows. (1) The distribution of the CR electrons is isotropic and depends only on the absolute value of the momentum $|\mathbf{p}|$. (2) Spatial averaged distribution is concerned. (3) Steadiness is assumed for simplicity; reality of this assumption

is discussed later. Thus, the distribution function has a form $f = f(p)$. The effect of the spatial diffusion is represented by the escape time formalism in the form of $-f(p)/T_d$, where the diffusion time is estimated by

$$T_d(p) = \frac{R^2}{D_0}, \quad (8)$$

where R is the spatial scale, i.e., the size of a radio halo.

The Fokker-Planck equation for the present model is, therefore,

$$\begin{aligned} \frac{1}{p^2} \frac{d}{dp} \left\{ D_{pp} p^2 \frac{df}{dp} - \dot{p}_{\text{loss}} p^2 f \right\} \\ - \frac{f}{T_d} + Q(p) = 0, \end{aligned} \quad (9)$$

where \dot{p}_{loss} indicates the momentum loss due to synchrotron radiation and inverse Compton effect, and $Q(p)$ is the particle injection rate at low energies. For the loss term, we use

$$\dot{p}_{\text{loss}} = -\frac{4\sigma_T}{3m_{e0}c^2} [U_{\text{mag}} + U_{\text{ph}}] p^2, \quad (10)$$

where $U_{\text{mag}} = B_0^2/(8\pi)$ is the energy density of the large-scale fields, and $U_{\text{ph}} \sim 4 \times 10^{-13}$ erg cm⁻³ is the energy density of 2.7 K background photons. For $Q(p)$, the mono-energetic injection at $\gamma = \gamma_i$ is assumed:

$$Q[p(\gamma)] = q_i \delta[p(\gamma) - p(\gamma_i)], \quad (11)$$

where q_i is the injection rate averaged over the radio halo region.

We rewrite equation (9) in terms of $\gamma \sim p/(m_{e0}c)$, in stead of p , and extract factors which are independent of γ to get

$$\begin{aligned} a_1 \gamma^w \frac{d^2 f}{d\gamma^2} + (w+2)a_1 \gamma^{w-1} \frac{df}{d\gamma} \\ + \frac{1}{\gamma^2} \frac{d}{d\gamma} \{a_2 \gamma^4 f\} - \frac{f[p(\gamma)]}{T_d} + Q[p(\gamma)] = 0 \end{aligned} \quad (12)$$

where,

$$a_2 = \frac{4\sigma_T}{3m_{e0}c} [U_{\text{mag}} + U_{\text{ph}}]. \quad (13)$$

The first term of equation (12) represents simple diffusion in the γ -space, while the second term causes the upward advection in the γ -space, i.e., the acceleration, with ‘velocity’ $\dot{\gamma}_{\text{accel}} = (w+2)a_1 \gamma^{w-1}$.

2.3. Characteristic Timescales

Two other characteristic timescales than T_d are used to normalize the equation: one is the acceleration time

$$T_a \sim \frac{\gamma}{\dot{\gamma}_{\text{accel}}} = \frac{\gamma^{2-w}}{(w+2)a_1}, \quad (14)$$

and the other is the momentum loss time

$$T_l \sim \frac{p}{|\dot{p}_{\text{loss}}|} = \frac{1}{a_2 \gamma}. \quad (15)$$

With the help of equations (4), (5) and (7), the spatial diffusion time (eq. [8]) is rewritten as

$$T_d = \frac{9R^2}{v_A^2} a_1 \gamma^{w-2}. \quad (16)$$

From equations (14) and (16), $T_d \propto 1/T_a$. This is because the larger the number of scattering is, the higher the acceleration rate is and the shorter the diffusion distance is. Thus, the shorter the acceleration time is, the larger diffusion time is. By using these three timescales, equation (12) can be rewritten as follows,

$$\begin{aligned} & \left(\frac{T_l}{T_a} \right) \left(\frac{\gamma^2}{w+2} \right) \frac{d^2 f}{d\gamma^2} + \left(\frac{T_l}{T_a} \right) \gamma \frac{df}{d\gamma} \\ & + \gamma^{-3} \frac{d}{d\gamma} (\gamma^4 f) - \left(\frac{T_l}{T_d} \right) f + T_l Q = 0. \end{aligned} \quad (17)$$

To understand the behavior of the solution, it is convenient to use a critical energy $m_{e0}c^2\gamma_c$ with which $T_a = T_l$. The Lorentz factor for the critical energy is

$$\gamma_c = \left[\frac{(w+2)a_1}{a_2} \right]^{\frac{1}{3-w}}. \quad (18)$$

By using γ_c , T_l/T_a and T_l/T_d can be written as follows

$$\frac{T_l}{T_a} = \left(\frac{\gamma}{\gamma_c} \right)^{w-3}, \quad (19)$$

$$\frac{T_l}{T_d} = \frac{(w+2)}{9} \left(\frac{v_A}{Ra_2} \right)^2 \gamma_c^{-2} \left(\frac{\gamma}{\gamma_c} \right)^{1-w}. \quad (20)$$

The large-scale-field strength and the spatial scale are given for each cluster, and hence a_2 is regarded as a constant. Therefore, the model free parameters are γ_c , w , and q_i .

When $w = 2$, the acceleration time (14) and the diffusion time (16) are independent of γ . In this case, the Fokker-Planck equation has an analytical solution (Schlickeiser 1984).

Schlickeiser et al. (1987) applied an approximated form of this analytical solution to the radio spectrum of the Coma halo. For solar flares, analytical solutions of the Fokker-Planck equation in general cases with $w \neq 2$ and finite T_d are discussed in Dröge & Schlickeiser (1986) and Steinacker, Jaekel, & Schlickeiser (1993). Park & Petrosian (1995) discussed the effects of the boundary conditions on the analytical solutions of the Fokker-Planck equation in general cases. However, these models cannot be applied to our model in their original forms because the synchrotron and the inverse Compton losses are neglected there.

One of our main purposes in this paper is to search the wider range of parameter space than the former work to investigate the radio spectra under various conditions. For this purpose, it is convenient to use numerical methods to solve the Fokker-Planck equation in general cases with $w \neq 2$ and the radiation loss. Equation (12) is one dimensional diffusion equation and is reduced to the algebraic equation of f by the differencing method. The obtained equation is numerically solved by the Gaussian elimination. The boundary conditions are $df/dp = 0$ at $p \rightarrow 0$ and $f \rightarrow 0$ at $p \rightarrow \infty$. The comparison between the obtained numerical solution and the analytic one for $w = 2$ suggests that the errors are $\sim 1\%$ in the present calculation.

2.4. Radio Flux

We calculate the radio spectrum from the obtained electron distribution function. The volume emissivity is given by

$$\epsilon_\nu = \int P_s(p, \nu) f(p) p^2 dp, \quad (21)$$

where P_s is the synchrotron radiation spectrum due to a single electron of momentum p :

$$P_s(p, \nu) = \frac{\sqrt{3}e^3}{m_{e0}c^2} B_0 x \int_x^\infty K_{\frac{5}{3}}(\eta) d\eta, \quad (22)$$

with $x = \nu/[3eB_0\gamma^2/(4\pi m_{e0}c)]$. The peak of this spectral distribution occurs at a frequency

$$\nu = \nu_B \gamma^2, \quad (23)$$

where $\nu_B = (0.29 \times 3eB_0)/(4\pi m_{e0}c)$. This relation (eq. [23]) defines a critical frequency ν_c corresponding to the critical energy $m_{e0}c^2\gamma_c$.

The radio flux is

$$S_\nu = \epsilon_\nu l \Omega_{\text{source}}, \quad (24)$$

where l is the source thickness, Ω_{source} is the solid angle of the radio halo. The radio flux is calculated numerically from the obtained distribution function to compare the observation. In §3, the radio flux is calculated for the radio halo in the Coma cluster, where we assume $l(=2R) = 600$ kpc, $\Omega_{\text{source}} = 30' \times 30'$ by adopting the size of the radio halo $R = 300$ kpc.

2.5. Model Parameters

The size of the radio halo $R = 300$ kpc, the gas number density $n = 10^{-3}$ cm $^{-3}$ are fixed for the Coma cluster, and we examine the case with two field strength $B_0 = 0.1$ and 1 μ G. The model free parameters are ν_c , w , and q_i .

The injection energy is assumed to be in the range 100 MeV $\lesssim E_i \lesssim 1$ GeV. In typical intracluster conditions, the cooling time of ~ 100 MeV electrons is fairly long (\sim a few Gyr). Thus, it is quite natural that there are abundant electrons with this energy range produced by some past active phenomena (Sarazin 1999). The source electrons may be produced at shocks in ICM (Takizawa & Naito 2000) or leaked out from radio galaxies, or normal galaxies. We choose the value of q_i so that the calculated net flux fits to the observed one.

3. RADIO SPECTRUM

3.1. Radio Spectrum and Alfvén Wave Energy Spectrum

Before comparison with the observations, we shall see parameter dependence of the solution to clarify the physical properties of the model. Four examples of the calculated radio spectrum are taken up in Figure 1 with different indices (a) $w = 2$, (b) $w = 2.8$, (c) $w = 4$, (d) $w = 6$ and with the fixed critical frequency at $\nu_c = 10$ MHz. The vertical axis of the figure is the radio flux in units of Jy, and the horizontal axis is the frequency in MHz. We assume $B_0 = 1$ μ G, and q_i is chosen so that the total luminosity in the 10 MHz–10 GHz range becomes $L \sim 10^{41}$ erg s $^{-1}$ for each example. The injection energy is $E_i \sim 100$ MeV which corresponds to the frequency $\nu \sim 0.05$ MHz in the models of $w = 2$ and 2.8 , and $E_i \sim 1$ GeV corresponding to $\nu \sim 5$ MHz in the models of $w = 4$ and 6 .

The shape of the distribution function is determined through competition between acceleration and loss. So, the useful parameter is T_l/T_a (see eq.[19]). The ratio T_l/T_a is proportional to γ^{w-3} , and therefore characteristic features of the obtained distribution function and, in turn, the shape of the radio spectrum depend on whether w is larger or smaller than 3. When $w < 3$, the injected electrons are scattered up to the critical energy $\gamma_c m_{e0} c^2$

because $T_a < T_l$ for $\gamma < \gamma_c$, whereas electrons diffusing out to energies higher than $\gamma_c m_{e0} c^2$ flow back in the energy space owing to the loss ($T_a > T_l$). Therefore, the electrons tend to gather around the critical energy $\gamma_c m_{e0} c^2$. For $w = 2$, we see in Figure 1a that the radio spectrum has the peak at ν_c because of this effect. For $w = 2.8$, the effect is attenuated by momentum space diffusion, but we can still see ‘the knee’ at ν_c .

When $w > 3$, electrons with energies smaller than $\gamma_c m_{e0} c^2$ essentially flow toward lower energies because $T_a > T_l$ for $\gamma < \gamma_c$. However, a small portion of the electrons is scattered out to energy larger than $\gamma_c m_{e0} c^2$. Once the energy reaches $\gamma_c m_{e0} c^2$, the electrons are accelerated because $T_a < T_l$. Moreover, the higher electron energy is, the more efficiently electrons are accelerated. As a result, the spectrum shows a concave shape around $\sim \nu_c$ as seen in Figures 1c and 1d.

We find that for $w > 3$ the radio spectrum becomes steeper as w is larger. Figures 1c and 1d show that the spectral index for $\nu > \nu_c$ is ~ 1 and ~ 2 when $w = 4$ and $w = 6$, respectively. This is due to strong energy dependence of the acceleration time. The net acceleration velocity in momentum space is $\dot{p} \sim p/T_a$ because T_a is shorter than T_l for $\nu > \nu_c$. For a steady state solution, the flow flux in momentum space is nearly constant,

$$4\pi p^2 \dot{p} f(p) = 4\pi p^3 \frac{f(p)}{T_a} \sim \text{constant}. \quad (25)$$

Hence, from equations (14) and (25), we obtain

$$f(p) \propto p^{-(w+1)}. \quad (26)$$

By using the monochromatic approximation, when the electron distribution function has power law index $\Gamma = w + 1$, the radio spectrum follows

$$S_\nu \propto \nu^{-(\Gamma-3)/2} = \nu^{-(w-2)/2}. \quad (27)$$

This relation explains the radio spectrum becomes steeper as w is larger, and $S_\nu \propto \nu^{-1}$ and $\propto \nu^{-2}$ when $w = 4$ and 6 , respectively.

When $w = 3$, T_a and T_l have the same γ -dependence, and therefore the ratio T_l/T_a is constant at any γ so that there is no critical frequency ν_c (i.e., γ_c): we find that $f(p)$ and the radio spectrum follows a single power law. The larger the value T_l/T_a , the flatter the spectral index is. When $T_l/T_a \sim 1$, the spectral index is $\alpha \sim 1$ in the 30 MHz–5 GHz range. When $w = 3$, the static solution to the Fokker-Planck equation without the diffusion loss term and the source term is $f \propto p^{-a_2/a_1} = p^{-5T_a/T_l}$ (Eilek & Henriksen 1984). For $T_a/T_l \sim 1$, $f \propto p^{-5}$, and in turn, $S_\nu \propto \nu^{-1}$ by using the monochromatic approximation.

If $w \neq 3$, the critical frequency ν_c is observable in a radio spectrum and characterize a radio spectrum. Determination of ν_c and the spectral index allows us to evaluate the energy spectrum of the turbulent Alfvén waves as shown in the next subsection and §4.

Table 1 shows the result of the parameter survey in the $\nu_c - w$ space, where w is in between 2 and 6, ν_c between 0.01 MHz and 10 GHz, $B_0 = 1 \mu\text{G}$, and $E_i = 100 \text{ MeV}$. When α falls in the observed range $1 \lesssim \alpha \lesssim 2$ in between 30 MHz and 5 GHz, the values are given in the columns. The model spectra which is too steep with $\alpha > 2$ or which is too flat with $\alpha < 1$ are represented by ‘S’ or ‘F’, respectively. When the spectrum has a peak in the observed frequency range, the model is denoted by ‘P’. When $w \geq 4$, the lower bound of the critical frequency is not known.

We also calculate for the models with $B_0 = 0.1 \mu\text{G}$. The relation between α and the model parameters are not altered significantly.

3.2. The Energy Density of Turbulent Alfvén Waves

The value $bB_0^2/(8\pi)$ means the energy density of the turbulent Alfvén waves for acceleration of the CR electrons radiating at $\nu \leq 5 \text{ GHz}$, when we assume $k_0 = k_{5\text{GHz}}$ in equation (3). The wave number $k_{5\text{GHz}} \sim 9 \times 10^{-15} B_{\mu\text{G}}^{3/2} \text{ cm}^{-1}$ is defined as the wave number resonating to the CR electrons radiating at $\nu = 5 \text{ GHz}$, which is similar to the observed maximum frequency. Figures 2a and 2b show the relation between b and w with $B_0 = 1 \mu\text{G}$ and $0.1 \mu\text{G}$, respectively. The solid line and the short-dashed line indicates, respectively, the lower and upper bound of b , which corresponds to the range $1 \lesssim \alpha \lesssim 2$.

The upper limit of the energy density of the turbulent Alfvén waves is the energy density of the large-scale-field $B_0^2/(8\pi)$. In figures 2a and 2b, the long-dashed line represents the upper limit $b = 1$. The shaded region indicates the allowed range of b and w . When $w < 4$ with $B_0 = 1 \mu\text{G}$, $b < 1$, i.e., the condition is met. However, when $w > 4$, the range of the parameters is constrained by the upper limit. When $B_0 = 0.1 \mu\text{G}$, the condition is met in the models with $w \lesssim 3.5$. In the models with $b > 1$, the energy density of the turbulent Alfvén waves exceeds $B_0^2/(8\pi)$. Such models are unrealistic.

As noted in the previous subsection, when $w > 4$, the lower bound of the critical frequency is not known. The values of the lower bound of the critical frequency determined by the constraint $b = 1$ are $3 \times 10^{-6} \text{ MHz}$ and 0.1 MHz for $w = 4$ and 5, respectively, when $B_0 = 1 \mu\text{G}$. When ν_c is less than the lower bound, the energy density of the turbulent Alfvén waves exceeds $B_0^2/(8\pi)$.

3.3. The Effect of Spatial Diffusion

The ratio T_l/T_d (eq.[20]) is rewritten as follows,

$$\frac{T_l}{T_d} \sim 3 \times 10^{-2}(w+2) \left(\frac{\gamma}{10^3}\right)^{1-w}, \quad (28)$$

where we use $B_0 = 1 \mu\text{G}$, $R = 300 \text{ kpc}$, the gas number density $n = 10^{-3} \text{ cm}^{-3}$, and $\gamma_c = 10^3$. Also, the ratio T_a/T_d is written as

$$\frac{T_a}{T_d} = \left(\frac{T_a}{T_l}\right) \left(\frac{T_l}{T_d}\right) = \left(\frac{\gamma}{\gamma_c}\right)^{3-w} \frac{T_l}{T_d} \sim 3 \times 10^{-2}(w+2) \left(\frac{\gamma}{10^3}\right)^{4-2w}. \quad (29)$$

The spatial diffusion term does not play a significant role in most cases because T_d is much longer than T_a and T_l within the observed frequency range ($\gamma > 10^3$). However, this is not the case when $w \lesssim 2$, which may be included in our parameter survey, e.g., $w = 5/3$ for Kolmogorov. If, for instance, $w = 2$, then $T_l/T_d \sim 0.1(\gamma/10^3)^{-1}$ and $(T_a/T_d) \sim 0.1$. Therefore, T_d is comparable to T_l at a energy range in which we are concern, and to T_a at all energies.

In §3.4 we search for the best fit model for the Coma radio halo and obtain the best model at $w = 2.8$, $\nu_c = 10 \text{ MHz}$ with $B_0 = 1 \mu\text{G}$. The spatial diffusion time of this best model is $T_d \sim 10^{11} \text{ yr}$ at $\gamma = 6.4 \times 10^4$ corresponding to 5 GHz. Since the spatial diffusion time is longer than the Hubble time, the distribution function does not reach to the steady state. However, the acceleration time and the energy loss time are shorter than the Hubble time, and therefore the distribution function becomes similar to the steady state solution quickly but only its normalization is different. The obtained physical quantities other than the injection rate are fairly valid. The injection rate q_i would be underestimated.

3.4. Comparison to the Observed Spectrum

We search for the best fit model for the Coma radio halo by the method of least squares. The average value of squared residuals is calculated as

$$J = \frac{1}{N_{\text{obs}}} \sum (\log S_{\text{cal}} - \log S_{\text{obs}})^2, \quad (30)$$

where S_{cal} is the calculated radio flux and S_{obs} is the observed one drawn from Deiss et al. (1997) and the number of the data points N_{obs} is 12. The radio flux (eq.[24]) is calculated with the solid angle $\Omega_{\text{source}} = 30' \times 30'$ and the source thickness $l (= 2R) = 600 \text{ kpc}$. (The distance to the Coma cluster is assumed to be 70 Mpc by adopting the Hubble constant

$H_0 = 100 \text{ km s}^{-1} \text{ Mpc}^{-1}$.) The obtained values of J with $B_0 = 1 \mu\text{G}$ are presented in Table 2. The best fit model ($J = 0.018$) is obtained when $\nu_c = 10 \text{ MHz}$ and $w=2.8$. Figure 3a shows the radio spectrum of this model with $B_0 = 1 \mu\text{G}$, and some physical quantities are summarized in Table 3. For the best fit model, $b \sim 1.7 \times 10^{-5}$ and the energy density of the turbulent Alfvén waves for the acceleration is $\sim 7 \times 10^{-19} \text{ erg cm}^{-3}$. (The factor b represents the fractional energy density of Alfvén waves accelerating the CR electrons radiating at $\nu \leq 5 \text{ GHz}$ [cf. §3.2].) This required energy density is much less than the energy density of the large-scale-field in the cluster $B_0^2/(8\pi) \sim 10^{-14} \text{ erg cm}^{-3}$.

Also, we obtain small values of J when $w = 4.5$ and $\nu_c \leq 1 \text{ MHz}$. The radio spectrum with $w = 4.5$ and $\nu_c = 1.0 \text{ MHz}$ is shown in Figure 3b. The required injection rate q ($= 4\pi p_i^2 q_i$) $\sim 3 \times 10^{-9} \text{ cm}^{-3} \text{s}^{-1}$ becomes very large when $E_i = 100 \text{ MeV}$. An injection at higher energy might resolve this difficulty.

Figure 3 shows that the spectra with a small value of $J \sim 0.02$, can have different shapes. If the spectrum shows exponential cut off such as shown in Figure 3a, the index w is smaller than 3, or otherwise, if the radio spectrum has a concave shape, the index w is larger than 3. When $w = 3$, the radio spectrum follows a single power law as mentioned in §3.1. Deiss et al. (1997) suggests that the value of the spatially integrated flux above 1.4 GHz is underestimated because of the small integration area. If more diffuse radio power is observed above 1.4 GHz, the model with $w > 3$ may well explain the observation. Further observation to determine the radio spectrum at higher frequencies set a stronger constraint on the energy spectrum of the turbulent Alfvén waves.

When $B_0 = 0.1 \mu\text{G}$, the models with $(w, \nu_c[\text{MHz}])=(2.8, 10)$, and $(4.5, 1)$ reproduce the observed spectrum. Table 3 shows that the required fractional magnetic energy density b is larger than that in the case of $B_0 = 1 \mu\text{G}$. When $w = 4.5$ and $\nu_c = 1.0 \text{ MHz}$, the energy density of the Alfvén waves for acceleration exceeds $B_0^2/(8\pi)$ as noted in §3.2.

4. DISCUSSION

4.1. The Energy Spectrum of Turbulent Alfvén Waves

Let us consider physical status of the turbulent Alfvén waves in our best fit model. Ruzmaikin & Shukurov (1982) gives the rate of energy-transfer via the nonlinear interaction among different wave numbers as

$$\left(\frac{dE}{dt} \right)_{\text{nl}} \sim \frac{P(k)^2 k^3}{\rho v_A}, \quad (31)$$

where ρ is the mean gas density. If the energy spectrum of the turbulent Alfvén waves is determined only through this energy cascade process, it becomes $P(k) \propto k^{-3/2}$ in a steady state because $(dE/dt)_{\text{nl}}$ is constant for k (Ruzmaikin & Shukurov 1982). However, this is significantly flatter than that in our best fit model whose exponent is -2.8 . Thus, other physical processes might work to steepen the Alfvén wave spectrum. Obviously, the Alfvén waves lose their energy through the particle acceleration. The CR electrons between p and $p + dp$ absorb the energy of Alfvén waves at the rate,

$$\begin{aligned} \left(\frac{dE}{dt} \right)_{\text{accel}} &= 4\pi p^2 (m_{e0}c^2) \dot{\gamma}_{\text{accel}} f(p) dp \\ &\sim 4\pi (m_{e0}c^2) p^3 \frac{\gamma}{T_a} f(p) \\ &\sim 4\pi m_{e0}^4 c^5 (w+2) a_1 \gamma^{w+2} f(p), \end{aligned} \quad (32)$$

where we use $dp \sim p$, $\dot{\gamma}_{\text{accel}} = \gamma/T_a$. We checked whether this plays a significant role or not in our best fit model. For simplicity, we approximate $P(k) \propto k^{-3}$ and $f(p) \propto p^{-6}$. In this case, $(dE/dt)_{\text{nl}} \propto k^{-3}$ and $(dE/dt)_{\text{accel}} \propto k^{-1}$ because the resonant wave number is proportional to p^{-1} . Therefore, the energy loss due to the particle acceleration is more significant in higher wave numbers and may be attributed to the spectral steepening. We checked if both terms are comparable to each other in the observed frequency range (30 MHz – 5 GHz), which corresponds to the wave number range of $(10^{-14} \sim 10^{-13}) B_{\mu\text{G}}^{3/2} \text{ cm}^{-1}$ (eq.[6]). The critical wave numbers k_t where $(dE/dt)_{\text{accel}} = (dE/dt)_{\text{nl}}$ are shown in Table 3 for our best fit models. They are certainly within or near the wave number range mentioned above. The obtained steep wave spectra, $w \sim 2.8$ and 4.5 for the Coma cluster and $w > 2.0$ in general, could be brought about by this effect. We suggest that time dependent and self-consistent calculations for non-linear wave-particle systems with back reaction of particle acceleration are necessary to investigate evolution of the systems.

Next, we make a crude estimate of $P(k)$ in $k < k_t$ and check the consistency of our consideration mentioned above. We adopt $P(k)$ of our best fit models for $k > k_t$ and assume $P(k) \propto k^{-\xi}$ for $k < k_t$. As a result, the broader band model power spectrum is,

$$P(k) = \begin{cases} P_t \left(\frac{k}{k_t} \right)^{-\xi} & (k_{\min} < k < k_t) \\ P_t \left(\frac{k}{k_t} \right)^{-w} & (k_t < k) \end{cases}, \quad (33)$$

where $P_t \equiv b_t (B_0^2/8\pi)(w-1)/k_t$ and k_{\min} is the wave number corresponding to the scale of the cluster, $k_{\min} \sim 10^{-24} \text{ cm}^{-1}$. Then, the total energy density of Alfvén waves M_{tot} is given by

$$M_{\text{tot}} = \frac{w-1}{\xi-1} b_t \frac{B_0^2}{8\pi} \left(\frac{k_t}{k_{\min}} \right)^{\xi-1} \left\{ 1 - \frac{w-\xi}{w-1} \left(\frac{k_t}{k_{\min}} \right)^{1-\xi} \right\}, \quad (34)$$

where we assumed $\xi > 1$. If we assume M_{tot} is as large as the energy density of the large-scale-field $B_0^2/(8\pi)$, then we obtain ξ with given k_t and b_t . When $B_0 = 1 \mu\text{G}$, $k_t \sim 10^{-14} \text{ cm}^{-1}$ and $b_t \sim 10^{-6}$, we have $\xi \sim 1.6$, which is close to the index of the energy spectrum, $3/2$, formed by the non-linear interaction. Therefore, this result is consistent with the previous picture of the non-linear interaction for $k < k_t$ and the acceleration reaction for $k > k_t$. When $B_0 = 0.1 \mu\text{G}$, $k_t \sim 10^{-15} \text{ cm}^{-1}$ and $b_t \sim 10^{-3}$, we have $\xi \sim 1.2$.

The rate of the energy transfer from $k_{30\text{MHz}}$ to higher wave numbers is estimated as $\varepsilon \sim [P(k_{30\text{MHz}})]^2 k_{30\text{MHz}}^3 / (\rho v_A)$. Table 3 shows that the values of ε are less than the thermal X-ray cooling rate except for the unrealistic case with $B_0 = 0.1 \mu\text{G}$, $w = 4.5$ and $\nu_c = 10\text{MHz}$. Therefore, even if the energy of the turbulent Alfvén waves goes into the thermal energy of the hot gas by the dissipation at higher wave numbers, the hot gas could not be heated up.

4.2. The Origin of the Turbulence

The energy transfer rate ε_0 at $k_{\text{min}} \sim 10^{-24} \text{ cm}^{-1}$ is estimated as $\varepsilon_0 \sim P_0^2 k_{\text{min}}^3 / \rho v_A \sim 10^{-31} B_{\mu\text{G}}^3 [\text{erg cm}^{-3} \text{ s}^{-1}]$, where $P_0 \sim B_0^2 / (8\pi k_{\text{min}})$. Thus, an energy input rate higher than ε_0 is necessary to excite and maintain the turbulence. It is certain that motion of galaxies through the intracluster medium can excite turbulent eddies. In this case, however, the energy input rate of the steady turbulence is

$$\epsilon_{\text{input}} \sim \rho v_0^3 / l_0 \sim 10^{-33} \text{ erg s}^{-1} \text{ cm}^{-3},$$

where $l_0 \sim 10 \text{ kpc}$ is a dimension of the galaxy, and $v_0 \sim 3.2 \text{ km s}^{-1}$ is the turbulent velocity at l_0 (Goldman & Rephaeli 1991). This input rate is insufficient for the required ε_0 . If the energy of the turbulence is input by the system of scale $R \sim 1 \text{ Mpc}$ with the velocity comparable to the sound velocity $v_s \sim 1000 \text{ km s}^{-1}$, the energy input rate is

$$\begin{aligned} \epsilon_{\text{input}} &\sim \frac{\rho v_s^2}{R/v_s} \\ &\sim 10^{-28} \left(\frac{n}{10^{-3} \text{ cm}^{-3}} \right) \left(\frac{v_s}{1000 \text{ km s}^{-1}} \right)^3 \\ &\quad \times \left(\frac{R}{1 \text{ Mpc}} \right)^{-1} \text{ erg s}^{-1} \text{ cm}^{-3}. \end{aligned} \quad (35)$$

This input rate is sufficient for the radio halo formation. A merging event between sub-structures can input the kinetic energy into the turbulence at this high rate. Moreover, cluster merger can produce seed CR electrons through 1st order Fermi acceleration at shocks in ICM (Takizawa & Naito 2000). Indeed, recent high resolution MHD simulations of cluster

mergers (Roettiger et al. 1999) show that the bulk flow is replaced by turbulent motion in the later stages of the merger.

4.3. The Supply of Cosmic Ray Electrons

We calculate the total number of the CR electrons N_{CR} from the luminosity and find $N_{\text{CR}} \sim 10^{60}$ for the Coma radio halo, where we adopt the luminosity $L_t \sim 10^{41} \text{ erg s}^{-1}$ (10 MHz $\leq \nu \leq 10 \text{ GHz}$), the spectral index $\alpha \sim 1.3$, and the magnetic field strength $B_0 \sim 1 \mu\text{G}$.

We examine how much the radio galaxy can supply the CR electrons. NGC4874 is one of the two dominant galaxies in the Coma cluster. The observed flux of the radio source associated with NGC4874 is $S_{408\text{MHz}} \sim 4 \times 10^{-24} \text{ erg cm}^{-2} \text{ s}^{-1} \text{ Hz}^{-1}$ at 408 MHz (Jaffe & Perola 1974). From the observed flux we calculate the number density of the CR electrons at the injection energy $\sim 100 \text{ MeV}$. For simplicity, we assume that the shape of the source is a sphere with a radius $r \sim 10 \text{ kpc}$, and that the radio spectrum follows a single power law with an index $\alpha \sim 0.5$. We also assume the magnetic field strength is $10 \mu\text{G}$. We find the number density $n_{\text{CR}} \sim 6 \times 10^{-11} \text{ cm}^{-3}$ at 100 MeV. The injection rate of the CR electrons leaked from the radio source is given by $\dot{n}_{\text{CR}} \sim 4\pi r^2 n_{\text{CR}} v_{\text{D}}$, where v_{D} is the diffusion velocity of the CR electrons. Taking $v_{\text{D}} \sim v_{\text{A}} \sim 700 \text{ km s}^{-1}$ gives an upper limit of the injection rate $\dot{n}_{\text{CR}} \lesssim 4 \times 10^{43} \text{ s}^{-1}$. When $\dot{n}_{\text{CR}} \sim 4 \times 10^{43} \text{ s}^{-1}$, the CR electrons in the radio halo are supplied in $N_{\text{CR}}/\dot{n}_{\text{CR}} \sim 7 \times 10^8 \text{ yr}$.

The merger shock acceleration supplies the CR electrons in the radio halo region. Takizawa & Naito (2000) assumed that the total kinetic energy of accelerated electrons is 5 % of the viscous energy, which is nearly equal to the energy of the shock heating, and they found that the luminosity of the synchrotron radio emission (10 MHz–10 GHz) is $\sim 10^{43} \text{ erg s}^{-1}$. We find the number of the CR electrons calculated from the luminosity is 5×10^{62} and sufficient for the observed radio halo, where we assume the magnetic field strength is $0.1 \mu\text{G}$ and the radio spectral index is 0.7. According to Takizawa & Naito (2000), the radio luminosity decreases after the most contracting epoch. We suggest that the turbulent Alfvén waves reaccelerate the CR electrons injected by the merger shock and maintain the radio halo.

5. SUMMARY

We have examined whether the particle acceleration by the turbulent Alfvén waves produces the radio halo in the cluster of galaxies. As a result, the energy spectrum of the

turbulent Alfvén waves reproducing the Coma radio spectrum has $w \sim 2.8$. It is most likely that the turbulence with sufficient energy for the radio halo formation is originated from some merging events between sub-structures. In our steady model, evolution of the turbulence and the magnetic fields with the cluster evolution is not considered. By considering effects of the cluster evolution, difference between the halo clusters and the non-halo clusters would be clarified. Such difference may also be indicated by observation of intracluster hard X-ray and thermal X-ray.

We thank T. Terasawa, M. Tosa, and M. Hattori for helpful suggestions. We would also like to thank the anonymous referee for his/her very useful comments.

REFERENCES

Berezinsky, V. S., Bulanov, S. V., Dogiel, V. A., Ginzburg, V. L., & Ptuskin, V. S. 1990, *Astrophysics of Cosmic Rays* (Amsterdam: North-Holland)

Blandford, R., & Eichler, D. 1987, *Phys. Rep.*, 154, 1

Blasi, P., & Colafrancesco, S. 1999, *Astropart. Phys.*, 12, 169

Blasi, P. 2000, *ApJ*, 532, L9

Deiss, B. M., Reich, W., Lesch, H., & Wielebinski, R. 1997, *A&A*, 321, 55

Dennison, B. 1980, *ApJ*, 239, L93

Dröge, W., & Schlickeiser, R., 1986, *ApJ*, 305, 909

Ebeling, H., Voges, W., Bohringer, H., Edge, A. C., Huchra, J. P., & Briel, U. G. 1996, *MNRAS*, 281, 799

Eilek, J. A., & Henriksen, R. N. 1984, *ApJ*, 277, 820

Felice, G. M., & Kulsrud, R. M. 2001, *ApJ*, 553, 198

Fukazawa, Y., Nakazawa, K., Isobe, N., Makishima, K., Matsushita, K., Ohashi, T., & Kamae, T. 2001, *ApJ*, 546, L87

Fusco-Femiano, R., Dal Fiume, D., Feretti, L., Giovannini, G., Grandi, P., Matt, G., Molendi, S., & Santangelo, A. 1999, *ApJ*, 513, L21

Fusco-Femiano, R., Dal Fiume, D., De Grandi, S., Feretti, L., Giovannini, G., Grandi, P., Malizia, A., Matt, G., & Molendi, S. 2000, *ApJ*, 534, L7

Giovannini, G., Feretti, L., Venturi, T., Kim, K. -T., & Kronberg, P. P. 1993, *ApJ*, 406, 399

Giovannini, G., Tordi, M., & Feretti, L. 1999, *New Astronomy*, 4, 141

Goldman, I., & Rephaeli, Y. 1991, *ApJ*, 380, 344

Hanisch, R. J. 1982, *A&A*, 116, 137

Holman, G. D., Ionson, J. A., & Scott, J. S. 1979, *ApJ*, 228, 576

Isenberg, P. A., 1987, *J. Geophys. Res.*, 92, 1067

Jaffe, W. J. 1977, *ApJ*, 212, 1

Jaffe, W., & Perola, G. C. 1974, *A&A*, 31, 223

Kim, K. -T., Kronberg, P. P., Dewdney, P. E., & Landecker, T. L. 1990, *ApJ*, 355, 29

Melrose, D. B. 1980, *Plasma Astrophysics* (New York: Gordon & Breach)

Park, B. T., & Petrosian, V. 1995, *ApJ*, 446, 699

Petrosian, V. 2001, *ApJ*, 557, 560

Ragot, B. R., & Schlickeiser, R. 1998, *Astropart. Phys.*, 9, 79

Rephaeli, Y. 1979, *ApJ*, 227, 364

Rephaeli, Y., Gruber, D. E., & Rothschild, R. E. 1987, *ApJ*, 320, 139

Rephaeli, Y., Gruber, D., & Blanco, P. 1999, *ApJ*, 511, L21

Roettiger, K., Stone, J. M., & Burns, J. O. 1999, *ApJ*, 518, 594

Roland, J. 1981, *A&A*, 93, 407

Ruzmaikin, A. A., & Shukurov, A. M. 1982, *Ap&SS*, 82, 397

Sarazin, C. L. 1999, *ApJ*, 520, 529

Schlickeiser, R. 1984, *A&A*, 136, 227

Schlickeiser, R. 1989, *ApJ*, 336, 243

Schlickeiser, R., & Miller, J. A. 1998, *ApJ*, 492, 352

Schlickeiser, R., & Rephaeli, Y. 1990, in *Proc. IAU Symp. 140, Galactic and Intergalactic Magnetic Fields*, eds. R. Beck et al. (Dordrecht: Kluwer), 487

Schlickeiser, R., Sievers, A., & Thiemann, H. 1987, *A&A*, 182, 21

Skilling, J. 1975, *MNRAS*, 172, 557

Steinacker, J., & Miller, J. A. 1992, *ApJ*, 393, 764

Steinacker, J., Jaekel, U., & Schlickeiser, R. 1993, *ApJ*, 415, 342

Takizawa, M., & Naito, T. 2000, *ApJ*, 535, 586

Terasawa, T. 1991, *Geophysical Monograph*, 61, 277

Wentzel, D. G. 1974, *ARA&A*, 12, 71

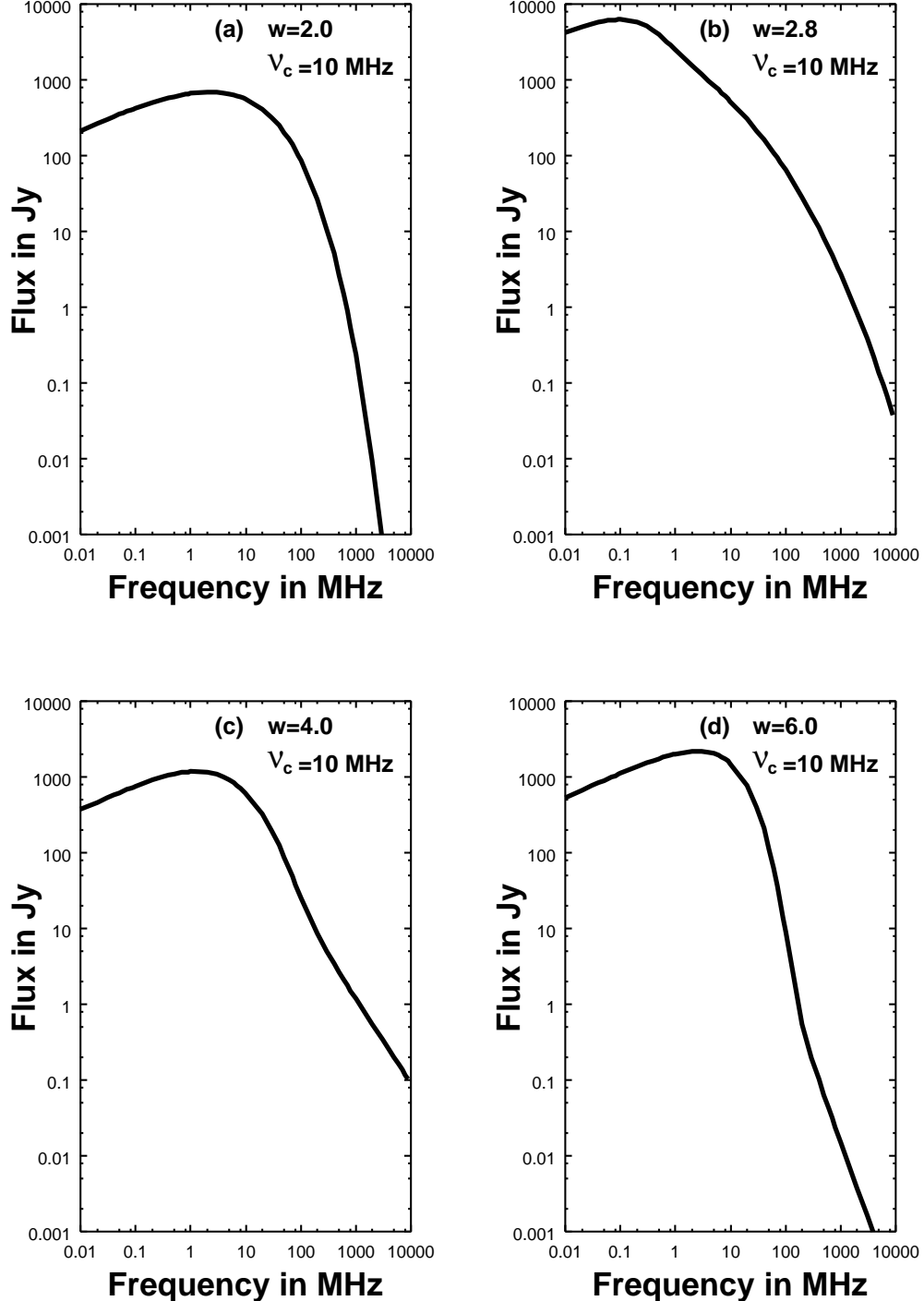


Fig. 1.— Calculated radio spectrum with $B_0 = 1 \mu\text{G}$, $R = 300 \text{ kpc}$, $\nu_c = 10 \text{ MHz}$ and various values of w . (a) $w = 2$; (b) $w = 2.8$; (c) $w = 4$; (d) $w = 6$. The radio spectrum shows convex and concave shape for $w < 3$ and $w > 3$, respectively.

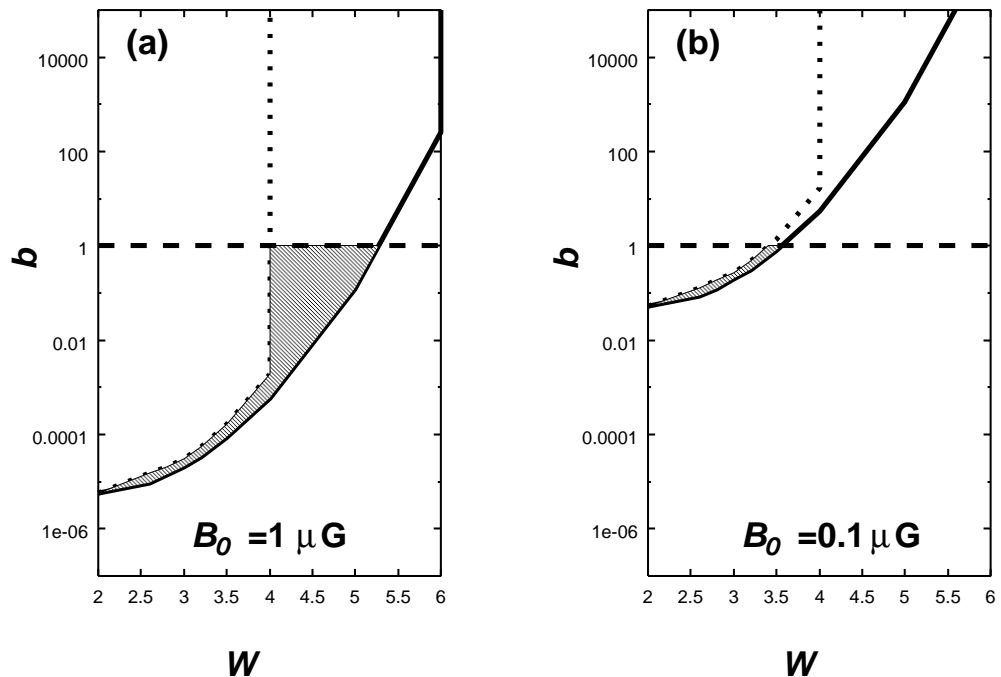


Fig. 2.— Relation between b and w . The solid line and the short-dashed line indicates, respectively, the lower and upper bound of b , which corresponds to the range $1 \lesssim \alpha \lesssim 2$. The long-dashed line represents the upper limit $b = 1$. The shaded region indicates the allowed range of b and w . In the models with $b > 1$, the energy density of the turbulent Alfvén waves exceeds $B_0^2/(8\pi)$.

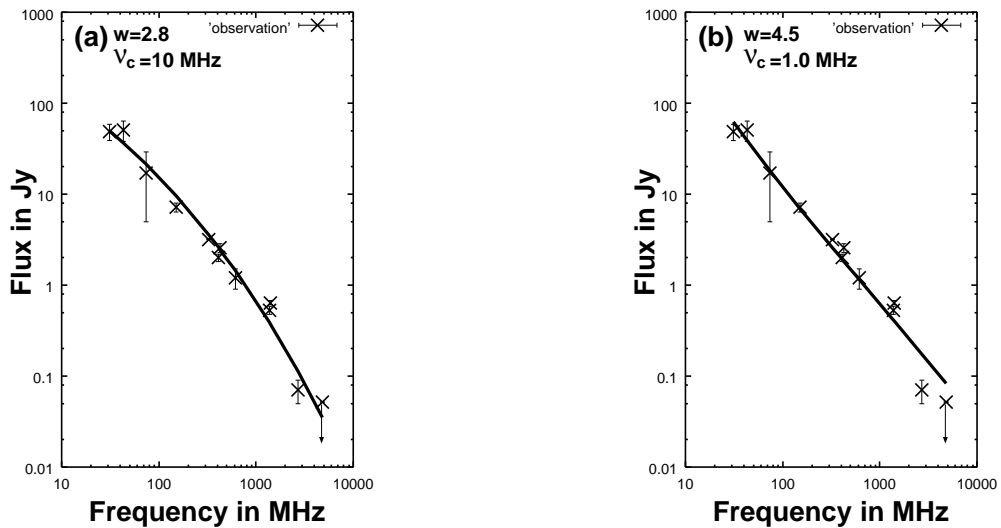


Fig. 3.— Two examples reproducing the observed radio spectrum. (a) $B_0 = 1 \mu\text{G}$, $\nu_c = 10$ MHz, $w = 2.8$; (b) $B_0 = 1 \mu\text{G}$, $\nu_c = 1$ MHz, $w = 4.5$; The observed intensity is drawn from Deiss et al. (1997).

Table 1. The calculated spectral index with w and ν_c .

ν_c (MHz)	w							
	2.0	2.6	2.8	3.2	3.5	4.0	5.0	6.0
10^4	P	P	F	S	S	S	S	S
10^3	P	F	F	2.07	S	S	S	S
10^2	1.02	0.97	1.03	1.35	2.61	S	S	S
10	S	1.90	1.44	0.96	1.16	1.79	S	S
1	S	S	2.03	F	0.88	1.08	1.54	S
0.1	S	S	S	F	F	1.02	1.50	2.00
0.01	S	S	S	F	F	1.00	1.50	2.00

Note. — Values in columns are α between 30 MHz and 5 GHz. Spectra of $\alpha > 2$ and spectra of $\alpha < 1$ are represented by the character ‘S’ and ‘F’, respectively. Spectra which has a peak in the observed frequency range is represented by ‘P’.

Table 2. The calculated values of J with w and ν_c .

ν_c (MHz)	w								
	2.0	2.6	2.8	3.2	3.5	4.0	4.5	5.0	6.0
10^4
10^3	0.71	0.49	0.30	0.33
10^2	0.14	0.11	0.075	0.053	0.91
10	1.4	0.14	0.018	0.11	0.070	0.17
1	...	1.6	0.20	0.18	0.13	0.063	0.027	0.036	...
0.1	1.0	0.22	0.16	0.077	0.028	0.030	0.20
0.01	0.24	0.18	0.082	0.028	0.029	0.20

Table 3. Model parameters reproducing the observed radio spectrum.

$(w, \nu_c [\text{MHz}])$	b^a	$bB_0^2/(8\pi)^b$ (erg cm^{-3})	q^c ($\text{cm}^{-3} \text{s}^{-1}$) $E_i=100 \text{ MeV}$	$E_i=1 \text{ GeV}$	k_t^d (cm^{-1})	b_t^e	ε^f ($\text{erg cm}^{-3} \text{s}^{-1}$)
$B_0 = 1 \mu\text{G}$							
(2.8, 10)	1.7×10^{-5}	6.8×10^{-19}	3.8×10^{-29}	2.3×10^{-30}	5.7×10^{-14}	6.1×10^{-7}	2.2×10^{-33}
(4.5, 1.0)	1.5×10^{-2}	6.0×10^{-16}	2.9×10^{-9}	4.1×10^{-29}	1.5×10^{-13}	8.1×10^{-7}	1.8×10^{-30}
$B_0 = 0.1 \mu\text{G}$							
(2.8, 10)	1.6×10^{-1}	6.2×10^{-17}	1.5×10^{-30}	1.4×10^{-30}	4.6×10^{-15}	1.0×10^{-3}	5.7×10^{-30}
(4.5, 1.0)	140	5.5×10^{-14}	1.1×10^{70}	2.5×10^{-26}	8.9×10^{-15}	8.3×10^{-4}	5.0×10^{-27}

^aThe value b is the fractional energy density of Alfvén waves above $k_{5\text{GHz}} = 9 \times 10^{-15} B_{\mu\text{G}}^{3/2} \text{ cm}^{-1}$.

^bThe energy density of Alfvén waves above $k_{5\text{GHz}}$.

^cThe values of the injection rate $q (= 4\pi p_i^2 q_i)$ for the steady state solution to reproduce the radio intensity.

^dThe value k_t is the wave number at which the energy loss rate due to the acceleration overcomes the energy transfer rate via the nonlinear interaction.

^eThe value b_t is the fractional energy density above k_t .

^fThe value ε is the energy transfer rate at $k_{30\text{MHz}}$.